arXiv:2502.04405v1 [cs.LG] 6 Feb 2025

FAS: Fast ANN-SNN Conversion for Spiking Large Language Models

Long Chen [1] **Xiaotian Song** [1] **Andy Song** [2] **BaDong Chen** [3] **Jiancheng Lv** [1] **Yanan Sun** [1]

Abstract

Spiking Large Language Models have been shown as a good alternative to LLMs in various scenarios. Existing methods for creating Spiking LLMs, i.e., direct training and ANN-SNN conversion, often suffer from performance degradation and relatively high computational costs. To address these issues, we propose a novel Fast ANN-SNN conversion strategy (FAS) that transforms LLMs into spiking LLMs in two stages. The first stage employs a full-parameter fine-tuning of pre-trained models, so it does not need any direct training from scratch. The second stage introduces a coarse-to-fine calibration method to reduce conversion errors and improve accuracy. Our experiments on both language and vision-language tasks across four different scales of LLMs demonstrate that FAS can achieve state-of-the-art performance yet with significantly reduced inference latency and computational costs. For example, FAS only takes 8 timesteps to achieve an accuracy of 3% higher than that of the OPT-7B model, while reducing energy consumption by 96.63%.

1. Introduction

Large Language Models (LLMs), with recent success in various applications, e.g., GPT-3 (Brown et al., 2020), LLaVA (Liu et al., 2024) and LLaMA 3 (Dubey et al., 2024), have become strong candidates in various tasks. However, all these models suffer from high energy consumption, mainly due to Floating-Point Multiplication and Addition (MAC) operations. For example, training GPT-3 consumes ∼1,287 MWh of energy (de Vries, 2023), which is equivalent to the annual energy consumption of 120 households. In recent years, a low-power alternative to vanilla LLMs, Spiking LLMs, have appeared, which are based on Spiking Neural Networks (SNNs), inspired by the spiking signalling mechanism of brain neurons (Bal & Sengupta, 2024; Zhu et al., 2023b). Through the energy-saving strategies of SNNs, i.e., computing with discrete binary spikes, the floating-point MAC of LLMs can be significantly reduced in Spiking LLMs, hence achieving low cost (Davies et al., 2018; Duan et al., 2024; Yao et al., 2024b).

[1]School of Computer Science, Sichuan University, China [2]School of Computing Technologies, Royal Melbourne Institute of Technology University, Australia [3]Institute of Artificial Intelligence and Robotics, Xi'an Jiaotong University, China.

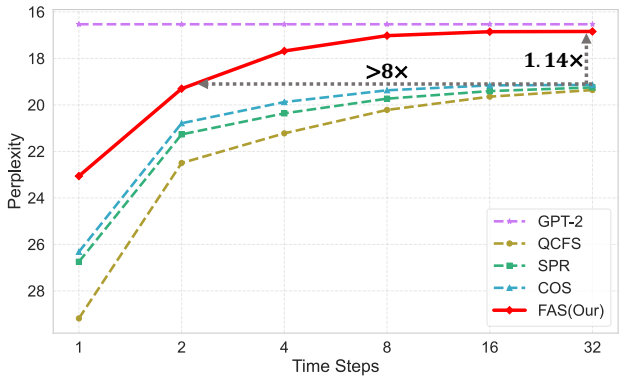

Figure 1. The performance of various ANN-SNN conversion methods on the GPT-2 for the WikiText-103 task.

Existing SNN-based approaches can be categorized into two different types: direct training and ANN-SNN conversion. The former typically uses backpropagation with surrogate gradient (Neftci et al., 2019; Zenke & Vogels, 2021; Lian et al., 2023). These approaches require training an SNN model from scratch, which is inherently time-consuming and resource-consuming, especially in the context of LLMs. Thus, the most common practice of these approaches only focus on training some components of LLMs on simple tasks (Yao et al., 2024a; Song et al., 2024). On the contrary, the latter approach, ANN-SNN conversion (Cao et al., 2015; Rueckauer et al., 2016; 2017), aims to convert ANN's analog neurons to spiking neurons, while eliminating the errors caused by the conversion. In this way, good-performing SNNs can be obtained with less or without a training process (Deng & Gu, 2021; Li & Zeng, 2022). ANN-SNN conversion has been successfully used in spiking Recurrent Neural Networks (RNNs) (Diehl et al., 2016) and spiking Convolutional Neural Networks (CNNs) (Lv et al., 2023) on complex tasks. However, existing ANN-SNN conversion methods cannot handle LLMs effectively, because the training strategy and scale of LLMs are significantly different

from those of RNN and CNN.

When dealing with LLMs, several problems arise. First, the training cost of LLMs is significantly higher than that of CNNs, making existing training-from-scratch conversion methods ineffective in the scenario. This limitation arises because these ANN-SNN conversion methods typically replace ANN activation functions with quantization-clipping functions to simulate spike rate discretization (Hao et al., 2023a; Wang et al., 2023) that do not fully utilize the pre-trained weights. As a result, they lead to high computational intensity when applied to LLMs. Second, the temporal errors in conversion on LLMs are larger than that on CNNs (Bu et al., 2023; Hao et al., 2023a;b), thereby resulting in severe performance degradation and inference latency. The reason is that the temporal errors accumulate layer by layer. Thus, with the increasing depth or scale of the model, the performance after ANN-SNN conversion deteriorates quickly. As illustrated in Figure 1, SOTA conversion methods suffer from a large performance gap with the GPT-2 baseline, especially when the time steps are small.

In this work, we propose a two-stage method for spiking LLMs, aiming for efficient yet effective ANN-SNN conversion. Specifically, the first stage involves a full-parameter fine-tuning of the pre-trained LLMs. This can eliminate the time-consuming process of training from scratch. In the second stage, a coarse-to-fine calibration method is introduced to eliminate temporal errors. The proposed method is termed FAS, Fast ANN-SNN conversion. Our contributions are summarized as follows:

- We propose FAS, a two-stage ANN-SNN conversion method for spiking LLMs. It achieves high-performance conversion with a low computational cost.
- We reveal that temporal errors are severe in conversion for spiking LLMs. To address this, a novel coarse-to-fine calibration component is introduced.
- We conduct experiments on both language and vision-language tasks across three LLMs and one multimodal LLM, showing that FAS can consistently achieve SOTA performance at low cost.

2. Related Works

Existing ANN-SNN conversion methods can be categorized into two groups: one-stage and two-stage conversion.

2.1. One-stage ANN-SNN Conversion

One-stage ANN-SNN conversion aims to directly convert ANN models to SNN models without any further optimization on the converted SNN models, e.g., fine-tuning. This type of method focuses on reducing the conversion as much as possible. For instance, Cao et al. (Cao et al., 2015) initially introduced the one-stage method by training ANNs with ReLU activation functions and then replacing these activations with spiking neurons. Based on this, Diehl et al. (Diehl et al., 2015) proposed model-based and data-based normalization to narrow the gap between ANN and SNN. Furthermore, Sengupta et al. (Sengupta et al., 2018) introduced scaling methods to normalize weights and thresholds of SNNs, improving the conversion performance. To further mitigate conversion loss, Rueckauer et al. (Rueckauer et al., 2016) and Han et al. (Han & Roy, 2020) introduced a "reset-by-subtraction" mechanism, which preserves temporal information and reduces information loss, enhancing precision during conversion. More recently, Bu et al. (Bu et al., 2022) analyzed conversion error and proposed the Quantization Clip-Floor-Shift activation function to replace ReLU in ANNs. This method can effectively approximate the SNN activation function and reduce conversion loss. One-stage ANN-SNN conversion has shown promising performance, however, it typically requires a large number of time steps to achieve SOTA performance. Note that 'time step' is the number of cycles used to analog the dynamic behavior of neurons, and plenty of time steps can cause the lengthy inference latency and huge energy consumption of the SNN model. Therefore, it is impractical to apply the one-stage methods to complex datasets and models with larger parameter scales, i.e., LLMs.

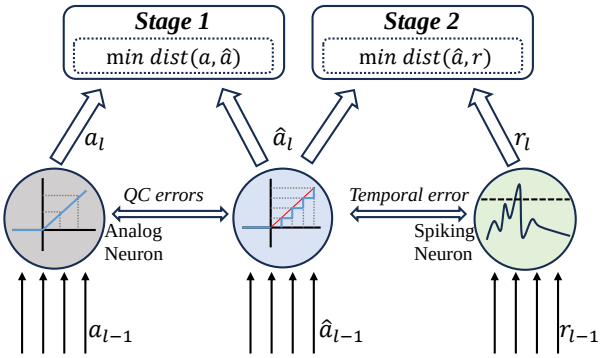

Figure 2. The overall framework of the proposed FAS method. *QC errors* is composed of the *quantization error* and the *clipping error*.

2.2. Two-stage ANN-SNN Conversion

Two-stage ANN-SNN conversion involves additionally optimizing the SNN converted by the one-stage methods to further to improve its performance. For example, SPR (Hao et al., 2023a) proposed an optimization strategy that uses residual membrane potential to reduce unevenness errors for converted SNN models. Similarly, COS (Hao et al., 2023b) optimized the converted SNN models by shifting the

initial membrane potential. However, SPR and COS require additional time steps to gather necessary prior information, which can reduce efficiency. To address this, LTL (Yang et al., 2022) introduced a local tandem learning rule, which can efficiently guide the training of the converted SNN models. In addition, EAC (Li et al., 2024) proposed a layer-wise calibration algorithm to optimize the converted SNN models. Specifically, this method first used grid search to find the optimal membrane threshold. Then, it adopted a greedy strategy for layer-by-layer validation and used stochastic gradient descent to update the parameters of the SNN model. However, LTL and EAC need to optimize all parameters of the converted SNN model. In comparison, the proposed FAS method only optimizes the membrane threshold and initial membrane potential. FAS is simpler and more effective than other peer competitors, especially for LLMs.

3. Preliminary

3.1. Analog Neuron Model for LLMs

LLMs are typically composed of Transformer architectures, which are structured layer by layer. The output a^l of the neurons in the l-th layer is achieved through a linear weighted combination followed by a nonlinear mapping:

$$a^l = f(W^l a^{l-1}), \tag{1}$$

where W^l is the weight matrix of the l-th layer, and $f(\cdot)$ is the nonlinear activation function, e.g., ReLU or GELU.

3.2. Spiking Neuron Model

For SNN, we follow the conversions (Diehl et al., 2015; Han et al., 2020; Deng & Gu, 2021) and consider the Integrate-and-Fire (IF) neuron model (Cao et al., 2015). Its kinetic behavior can be represented by Eq. (2):

$$v^l(t) = v^l(t-1) + W^l S^{l-1}(t)\theta^{l-1} - S^l(t)\theta^l, \tag{2}$$

where $v^l(t)$ represent the membrane potential at time steps t in the i-th layer. W^l and θ^l are the weight matrix and firing threshold of the IF neuron, respectively. $S^l(t)$ denotes the transmission of discrete spikes at the l-th layer at time steps t. Note that when $v^l(t-1) + W^l S^{l-1}(t)\theta^{l-1}$ exceeds the threshold θ^l, the IF neuron is activated, so $S^l(t)$ equals 1. Otherwise, the IF neuron is inhibited and $S^l(t)$ equals 0.

3.3. Conversion Error of ANN-to-SNN

ANN-SNN conversion aims to establish a consistent relationship between the analog neurons and the spike rates of IF neurons. The spike rate $r^l(T)$ can be represented as Eq. (3) (more details are in **Appendix A**):

$$r^l(T) = \text{clip}(\frac{\theta^l}{T}\left\lfloor \frac{TW^l r^{l-1}(T) + v^l(0)}{\theta^l} \right\rfloor, 0, \theta^l). \tag{3}$$

Specifically, the conversion can be achieved by mapping the activation value a^l of ANNs (see Eq. (1)) to the spike rate r^l of SNNs (see Eq. (3)). However, the conversion process still has three types of conversion errors: ① *Quantization error:* The spike rate is a discrete distribution, with values occurring at regular intervals of θ/T. When $a^l \in \left[k\theta^l/T, (k+1)\theta^l/T\right]$, it is mapped to $k\theta^l/T$. The discrepancy $a^l - k\theta^l/T$ is a source of errors. ② *Clipping error:* This is caused by the different value ranges of ANN and SNN. Specifically, when $a^l \in [0, a_{max}]$ and $r^l \in [0, \theta^l]$, where a_{max} denote the max value in a^l, the value $a^l \in [\theta^l, a_{max}]$ will be all mapped to θ^l, also generating errors. ③ *Temporal error:* It refers to the inconsistency between a^l and r^l due to the fluctuation in the temporal sequences of spike arrivals in activation layers. This variation can result in a higher or lower number of spikes than expected, resulting in poor performance.

4. Methodology

4.1. Overall Framework

As discussed in Section 3.3, the *quantization errors* and *clipping errors* come from the process of discretizing the continuous ANN activation function, and the *temporal errors* are caused by using the disordered temporal sequences to generate spikes. The proposed FAS method is tailored for eliminating these errors in LLMs, which can secure the high-performance and low-energy spiking LLMs. Specifically, the overall framework of FAS is shown in Figure 2, consisting of two stages. The arrow between the gray circle on the left and the middle blue circle represents two types of errors, *Quantization error* and *Clipping error*, respectively, totally denoted as *QC errors*. The arrow between the middle and right circles represents *Temporal errors*. These errors are addressed in the two stages of FAS. More specifically, ***Stage 1*** addresses *QC errors* through full- parameter fine-tuning. ***Stage 2*** employs a layer-wise and neuron-wise coarse-to-fine calibration optimization strategy to minimize *Temporal errors*. The details of the algorithm are presented in **Appendix B**, and the two stages of FAS will be discussed in the next sections.

4.2. *Stage 1:* Eliminating QC Errors

Inspired by Eq. (3), we select a continuous step function to replace the activation function in ANN to approximate the activation function of SNNs, thereby eliminating *QC errors*. In this paper, we consider Quantization Clip-Floor-Shift (QCFS) function (Bu et al., 2022), which is described as:

$$a^l = f(W^l a^{l-1}) = \text{clip}(\frac{\lambda^l}{L}\left\lfloor \frac{W^l a^{l-1} L}{\lambda^l} + \frac{1}{2} \right\rfloor, 0, \lambda^l), \tag{4}$$

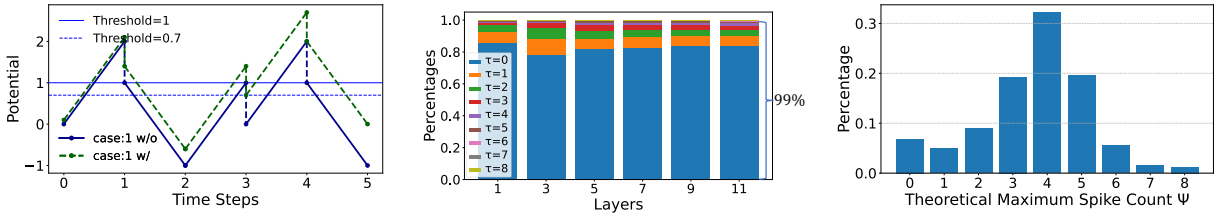

(a) Observation 1: 'w/' and 'w/o' denotes the case with and without optimization.

(b) Observation 2: The distribution of theoretical spike counts with layers.

(c) Observation 3: The distribution of theoretical maximum spike counts.

Figure 3. Illustration of our observations.

where λ^l is maximum value in ANN activation function, mapped to the thresholds θ^l in SNN. L refers to the number of simulation steps. In contrast, existing methods, including QCFS, focus on eliminating *QC errors* that need to be trained from scratch to get the initial ANN model (Bu et al., 2023; Wang et al., 2023; Hao et al., 2023a). However, it is time-consuming and impractical for LLMs. To address this, we novelty choose the pre-trained LLMs as the initial model that can effectively reduce the computational cost.

4.3. Observations from Post-Stage-1 Analysis

To better understand the source of the remaining error, i.e., *temporal error*, we conducted an in-depth analysis.

Definition. We define *Theoretical Maximum Spike Count* ψ^i of neuron i in the l-th layer as max of *Theoretical Spike Count* τ_{theor} during the interval $[0, T]$ for all data, that is:

$$\psi^i = \text{Max}(\tau_{theor}) = \text{Max}(\frac{a^i T}{\lambda^i}), \tag{5}$$

where a^l/λ^l represents the normalized output in the ANN. τ_{theor} denotes the number of spikes needed by an SNN neuron to accurately represent a^l. ψ^i indicates that the τ_{theor} in the i-th neuron will not exceed ψ^i. If the spike count in the SNN matches τ_{theor}, the conversion error would be zero. However, due to the *temporal error*, the actual spike count typically does not equal τ_{theor}. Based on the definitions, we have made the following three observations:

Observation 1. By lowering the thresholds when $\tau_{theor} < T$, the *temporal error* can be reduced.

The maximum activation value θ^l in the SNN is aligned with the upper activation bound λ^l of the ANN, thereby eliminating clipping error. However, when a^l is lower than θ^l, θ^l can be set within the range $[a^l, \theta^l]$ without affecting the firing rate mapping to a^l, provided that other data is not considered. Furthermore, *temporal error*, caused by firing more or fewer spikes than expected, can be expressed as:

$$\text{Error}_T = \frac{|\tau_{real} \cdot \theta^l - \tau_{theor} \cdot \lambda^l|}{T}, \tag{6}$$

where τ_{real} represents the number of spikes in practice. As θ^l decreases, the *temporal error* decreases as well. Lowering the threshold θ^l may slightly affect the firing rate representation, but this can be mitigated by optimizing initial membrane potentials. This effect is minor compared to the reduction in *temporal error*. The following example illustrates this point.

Consider two pre-synaptic neurons in the $(l-1)$-th layer connected to a postsynaptic neuron in the l-th layer, as shown in Figure 3(a), denoted as case 1. Note that we assume $\theta^l = 1$, $\lambda^l = 1$, $\tau_{theor} = 2$, and $T = 5$ in case 1. If the pre-synaptic neurons fire at $t = 1, 3, 4$ and $t = 2, 5$, respectively, the postsynaptic neuron will fire three spikes at $t = 1, 3, 4$. Thus, the number of the spikes, i.e., τ_{real}, is three. Based on Eq. (6), the *temporal error*, i.e., Error_T, is 0.2. By lowering the SNN thresholds θ^l to 0.7 and resetting the initial membrane potentials, the *temporal error* is reduced to 0.02.

Observation 2. $\tau_{\text{theor}} \leq T/2$ in 99% of the cases in each layer, lowering the threshold in each layer can effectively decrease *temporal error*.

We further investigate the distribution of theoretical spike count τ_{theor} in each layer. Figure 3(b) shows the τ_{theor} distribution for the converted GPT-2 model on WikiText-103 with 8 time steps. It is observed that $\tau_{\text{theor}} \leq 4$ accounts for 99% of cases, while $\tau_{\text{theor}} \geq 5$ accounts for only 1%. This indicates that neurons in the SNN typically need to fire at most 4 spikes to represent ANN activation values. The range of r^l is $[0, \tau_{theor}\theta^l/T] = [0, \theta/2]$. Based on this, we can lower the threshold to within $[\theta/2, \theta]$. Combined with **Observation 1**, this effectively reduces *temporal error* for all neurons. For example, decreasing the threshold in each GPT-2 layer to 60% of its original value shows performance improvement. Detailed analyses are in the ablation study.

Observation 3. $\psi^i > T/2$ also occupies a significant portion, necessitating threshold optimization for each neuron to achieve better performance.

We investigate the distribution of the theoretical maximum spike count ψ^i for each neuron, excluding the top 1% of τ_{theor} cases. As shown in Figure 3(c), ψ^i varies among neurons, with most being less than T. This suggests that lowering the threshold, as **Observation 2**, effectively reduces *temporal error*. However, unlike **Observation 2**, where $\tau_{\text{theor}} > T/2$ was rare (1%), many neurons have $\psi^i > T/2$. Thus, reducing the threshold in each layer too much jeopardizes the performance of these neurons, while reducing it slightly will not sufficiently decrease the *temporal error*. Thus, optimizing the threshold of each neuron is necessary.

In summary, our post-stage-1 study shows that lowering the threshold can reduce *temporal error*. The second stage, which is detailed next, is designed based on this observation.

4.4. *Stage 2:* Eliminating Temporal Error

To minimize *temporal error*, we first reduce the overall *temporal error* through *layer-wise calibration* of the thresholds and initial membrane potentials. Then, we perform *neuron-wise calibration* to optimize each neuron.

Layer-wise calibration (LWC): As shown in **Observation 2**, adjusting the threshold and initial membrane potentials in each layer can reduce *temporal error*. Thus, we optimize the thresholds and initial membrane potentials as:

$$\widehat{\theta}^l = \alpha^l * \theta^l, \widehat{v}(0)^l = \beta^l * \widehat{\theta}^l, \tag{7}$$

where θ^l is the threshold of the l-th layer, $v(0)^l$ is the initial membrane potential of the l-th layer; α^l and β^l are their optimization weights; $\widehat{\theta}^l$ and $\widehat{v}(0)^l$ represent the optimized thresholds and initial membrane potentials, respectively. The optimal value of α^l can be determined by analyzing the distribution of theoretical spike counts in the training set.

Neuron-wise calibration (NWC): For each neuron, we set a trainable threshold θ_i^l and initial membrane potential $v(0)_i^l$, with initial values set after layer-wise calibration. Using the ANN as a guide, we input the same data into both the ANN and SNN for forward propagation, minimizing the distance between the firing rate of each SNN neuron and the output of the corresponding ANN neuron. We freeze all model parameters except the thresholds and initial membrane potentials of the IF neurons, then update these parameters for each neuron to achieve neuron-wise optimization. Due to the discrete and non-differentiable nature of spikes, standard backpropagation cannot be used here, so we employ BPTT (Lee et al., 2016; Wu et al., 2017) for calibration.

Next, the proposed loss functions used for backpropagation are discussed, i.e., *activation align loss* and *logits loss*.

Activation align loss: To minimize the *temporal error* of SNN, the firing rate of IF neurons should align with the activation values of the ANN. The loss function can be described as:

$$L_i^{al} = mse(a_i^l, r_i^l) = mse(f(W^l a^{l-1}), \frac{\sum_{t=1}^{\rho} s_i^l \theta_i^l}{T}), \tag{8}$$

where ρ denoted the time steps used for calibration. a_i^l is the output of the i-th neuron in the l-th layer, while r_i^l signifies the fire rate of the i-th neurons in the l-th layer.

Logits loss: Following (Hinton et al., 2015), we use logits loss, which lets the SNN learn the prediction distribution of the ANN. To measure the distance between two distributions, we choose KL-divergence:

$$L_{logits} = -\sum_i^c \text{Softmax}(\tfrac{a_i}{T})\log(\text{Softmax}(\tfrac{r_i}{T})), \tag{9}$$

where T is the temperature parameter, a_i represents the output of the ANN, r_i represents the spike fire of the SNN, and c represents the number of classes. Therefore, the total loss contains two terms:

$$L_{all} = \lambda_1 \sum_i L_i^{al} + \lambda_2 L_{logits}, \tag{10}$$

where λ_1 and λ_2 are the hyper-parameters that control the weight of activation align loss and logits loss, respectively.

5. Experiments

5.1. Datasets & Baselines & Settings

To evaluate the proposed FAS method, we selected various language and vision-language tasks. More details are presented in **Appendix C**. In addition, we chose various SOTA models, including LLM and multimodal LLM with 7B parameters, as the peer competitors, and their details are provided in **Appendix D**. Note that the experiment settings are also presented in **Appendix E**.

5.2. Experiments on NLU Tasks

Performance Analysis on Bert: To the best of our knowledge, this study is the first to report and analyze the performance of an ANN-SNN conversion-based spiking LLM on multiple tasks. Table 1 compares FAS with other SOTA models in NLU tasks using BERT, demonstrating FAS achieves new SOTA performance across seven text classification datasets. Specifically, on the QNLI and MRPC tasks, FAS surpasses other directly trained SNN models (the second block of Table 1) by at least 5%. On the QQP and STS-B tasks, SNN-TextCNN fails to converge, while FAS performs significantly well. Compared to other ANN-SNN methods (the third block of Table 1), FAS outperforms the QCFS by 10% on the RTE task, the SRP by 5.21% on the MNLI-m task, and the COS by 6.36% on the MRPC task. Notably, FAS achieves superior performances with time steps of only 4, indicating the low latency of the model.

Table 1. Comparing FAS with SOTA models of BERT on the GLUE evaluation set. *S* denotes whether an SNN or not. *T* is the time steps. * denotes non-convergence. † indicates additional time steps required to gather the necessary prior information. Accuracy is the metric for QQP, MNLI-m, SST-2, QNLI, RTE. MRPC combines accuracy and F1 scores. STS-B uses the Pearson/Spearman correlation. The three blocks group models of non-SNN, direct trained and ANN-SNN converted.

Model	*S*	*T*	**QQP**	**MNLI-m**	**SST-2**	**QNLI**	**RTE**	**MRPC**	**STS-B**
BERT (Devlin et al., 2019)	✗	N/A	90.71	83.91	92.32	90.66	65.70	84.07/88.85	88.64/88.48
CBoW (Wang et al., 2018)	✗	N/A	75.00	57.10	79.50	62.50	71.90	75.00/83.70	70.60/71.10
BiLSTM (Wang et al., 2018)	✗	N/A	85.30	66.70	87.50	77.00	58.50	77.90/85.10	71.60/72.00
BiLSTM + Attn, CoVe (Wang et al., 2018)	✗	N/A	83.50	67.90	89.20	72.50	58.10	72.80/82.40	59.40/58.00
GenSen (Subramanian et al., 2018)	✗	N/A	82.60	71.40	87.20	62.50	78.40	80.40/86.20	81.30/81.80
SNN-TextCNN (Lv et al., 2023)	✓	50	0.00*	64.91	80.91	64.91	47.29	-/80.62	0.00*/-
spikeBERT (Lv et al., 2024)	✓	4	68.17	71.42	85.39	66.37	57.47	-/81.98	-/18.73*
SpikeLM (Xing et al., 2024)	✓	4	-	77.10	87.00	85.30	69.00	-/85.70	84.90/-
SpikingBERT (Bal & Sengupta, 2024)	✓	60	86.82	78.10	88.19	85.20	66.06	79.17/85.15	82.20/81.90
SPR (Hao et al., 2023a)	✓	8 (16†)	87.48	77.56	90.48	87.75	64.98	78.68/85.76	86.71/86.50
QCFS (Bu et al., 2023)	✓	8	88.42	79.57	89.91	86.80	56.68	78.92/85.37	86.18/85.82
COS (Hao et al., 2023b)	✓	8 (8†)	88.85	79.91	89.79	87.37	63.18	79.66/86.33	86.49/86.23
FAS (BERT)	✓	**4**	**90.38**	**82.77**	**91.17**	**90.13**	**66.06**	**86.02/90.22**	**87.46/87.26**

Table 2. Energy efficiency analysis of FAS on the QQP task of BERT model. Also, SRP and COS need an additional 16 time steps to gather the necessary prior information. ↑ and ↓ denote the performance is better or worse than the baseline BERT model, respectively.

T	**FAS**		**QCFS**		**SRP**		**COS**	
	Accuracy	**Energy (%)**	**Accuracy**	**Energy (%)**	**Accuracy**	**Energy (%)**	**Accuracy**	**Energy (%)**
N/A (BERT)	90.66	100	90.66	100	90.66	100	90.66	100
16	**90.75** (↑ 0.09)	8.42	87.53 (↓ 3.13)	2.50	87.28 (↓ 3.38)	5.46	87.31 (↓ 3.35)	4.98
8	90.20 (↓ 0.46)	4.56	86.84 (↓ 3.82)	1.28	87.41 (↓ 3.25)	4.11	86.82 (↓ 3.84)	3.77
4	90.38 (↓ 0.28)	3.14	85.01 (↓ 5.56)	0.65	87.15 (↓ 3.51)	3.42	87.31 (↓ 3.35)	3.16
2	89.69 (↓ 0.97)	1.88	82.19 (↓ 8.47)	0.32	86.23 (↓ 4.43)	3.05	86.66 (↓ 4.00)	2.84
1	88.94 (↓ 1.72)	1.14	81.55 (↓ 9.11)	**0.12**	84.94 (↓ 5.72)	2.84	84.81 (↓ 5.85)	0.31

Table 3. Comparing the accuracy of zero-shot tasks between FAS and SOTA OPT models.

Model	*S*	*T*	**Energy (%)**	**PIQA**	**ARC**	**OpenbookQA**	**Winogrande**	**COPA**	**WSC**	**RTE**
OPT-7B (Zhang et al., 2022)	✗	N/A	100	76.26	65.57	27.60	65.43	81.00	82.05	55.25
FAS (OPT-7B)	✓	**8**	3.37	72.74	63.97	27.60	60.30	**84.00**	77.29	53.07
	✓	16	5.06	73.23	**64.73**	27.00	**60.38**	83.00	**77.66**	**55.60**
	✓	32	8.41	**74.05**	64.60	**27.80**	60.06	82.00	77.29	55.23

Energy Analysis on Bert: To justify the great energy efficiency of FAS, we quantify the energy reduction of FAS under different time steps on BERT. As shown in Table 2, FAS can effectively reduce the energy consumption yet with the SOTA performance across all time steps. Note that the performance of FAS even exceeds the baseline BERT model with only 8.42% energy consumption. In addition, compared to others, i.e., QCFS, SRP, and COS, FAS has fewer time steps under similar energy consumption. This indicates that FAS has a faster inference speed than others, especially when deploying on hardware. Note that the details of the energy consumption are described in **Appendix F**.

Performance & Energy Analysis on OPT-7B: We also conducted the experiments on the larger model, i.e., OPT-7B, to further justify the effectiveness of FAS. As presented in Table 3, we compared the performance of OPT and the spiking OPT converted by FAS under different time steps. The results show that FAS, as well as or outperforming the original OPT-7B model across different tasks. Specifically, in OpenBookQA and COPA, FAS under 8 time steps achieved the same or higher performance than OPT. In the RTE task, FAS with 16 time steps surpassed the performance of OPT. Additionally, FAS can significantly reduce energy consumption across the different time steps on OPT-7B.

5.3. Experiments on NLG Tasks

Table 5 presents the results of FAS using the GPT-2 architecture on the Enwik8 and WikiText-103 datasets. It outperforms all other methods with low latency inference (T=16). For Enwik8, FAS achieves 0.968 BPB, whereas the QCFS and SRP methods reach 1.016 and 1.014 BPB at 32 time steps. COS reaches 1.01 BPB at 16 time steps, but re-

Table 4. Compare the performance of FAS and SOTA multimodal LLMs on different vision-language tasks.

Model	S	T	HallusionBench Question Pair Acc.	HallusionBench Figure Acc.	HallusionBench Question Acc.	BLINK Test	MMMU Val
MiniGPT-4-v2-7B (Zhu et al., 2023a)	✗	N/A	8.79	10.12	35.78	34.6	-
Qwen-VL-8B (Bai et al., 2023)	✗	N/A	5.93	6.65	39.15	-	-
Claude 3 (Sonoda et al., 2024)	✗	N/A	21.76	28.61	56.86	44.1	50.2
PailGamme-3B (Beyer et al., 2024)	✗	N/A	22.63	21.96	51.84	38.29	32.88
LLaVA-1.5-7B (Liu et al., 2024)	✗	N/A	15.31	20.87	52.78	41.22	33.66
FAS (PailGamme-3B)	✓	**8**	**25.27**	**23.41**	**53.52**	**38.92**	**29.67**
FAS (LLaVA-1.5-7B)	✓	**8**	**18.68**	**19.78**	**51.41**	**40.37**	**31.33**

Table 5. Comparing FAS with SOTA GPT models on the NLG dataset. **'En8'** stands for Enwik8, with BPB as the metric. **'WT'** is WikiText-103 using perplexity. The lower the better for both metrics. ** denotes the absence of time steps and fine-tuning.

Model	S	T	En8	WT
GPT-2 (Radford et al., 2019)	✗	N/A	0.96	16.53
Transformer-SSA (Hussain, 2023)	✗	N/A	1.02	16.91
AstroSNN (Shen et al., 2023)	✓	$-^{**}$	1.14	32.97
spikeGPT (Zhu et al., 2023b)	✓	1024	1.26	18.01
SPR (Hao et al., 2023a)	✓	32 ($16^{\dagger}$)	1.01	19.24
QCFS (Bu et al., 2023)	✓	32	1.02	19.36
COS (Hao et al., 2023b)	✓	16 ($16^{\dagger}$)	1.01	19.15
FAS (GPT-2)	✓	**16**	**0.97**	**16.84**

Table 6. Impact of the parameter ρ in GPT-2. Baseline refers to the SNN without Stage 2 optimization.

T	$\rho=1$	$\rho=2$	$\rho=4$	$\rho=6$	$\rho=8$
N/A (GPT-2)	16.39	16.39	16.39	16.39	16.39
1	**23.06**	24.79	30.01	34.37	39.30
2	20.79	**19.30**	19.84	20.79	21.98
4	19.75	18.20	**17.68**	17.78	18.01
6	19.42	17.91	17.32	**17.23**	17.29
8	19.30	17.79	17.21	**17.05**	19.03
16	19.17	17.67	17.09	16.93	**16.84**
32	19.13	17.64	17.09	16.94	**16.83**

quires additional time steps for prior information. Moreover, on WikiText-103, FAS achieves a perplexity (PPL) of 16.84, while SpikeGPT reaches 18.01 PPL at 1024 time steps. FAS also outperforms other ANN-SNN conversion methods (the third block of Table 5) by a large margin. Note that FAS also has a high energy efficiency on GPT-2 across different time steps, and the details are provided in **Appendix F**.

5.4. Experiments on Vision-Language Tasks

To validate the generalization of FAS, we conducted experiments on the multimodal Pailgemma-3B and LLaVa-1.5-7B. As shown in Table 4, FAS outperformed the baseline Pailgemma-3B model on the HallusionBench and BLINK benchmarks with 8 time steps. Moreover, despite having only 3B parameters, FAS exceeded the performance of several larger 7B models, including MiniGPT-4 and Qwen-VL-8B, across all tasks. Additionally, for LLaVa-1.5-7B, FAS achieved high accuracy, with performance only 0.8 lower than the original LLaVa-1.5-7B model, using only 8 time steps. Moreover, FAS outperformed both MiniGPT-4 and Qwen-VL-8B on all tasks, and exceeded the performance of Pailgemma-3B on the BLINK task with 8 time steps.

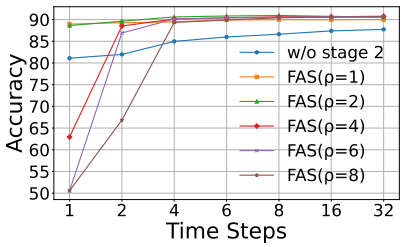

(a) BERT on QNLI.

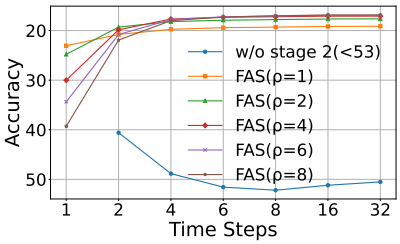

(b) GPT-2 on WikiText-103.

Figure 4. Impact of parameter ρ on BERT and GPT-2.

5.5. Ablation Study and Impact of Hyper-Parameters

5.5.1. Parameter ρ :

We investigate the impact of the hyperparameter calibration steps ρ in ***Stage 2*** of FAS. Figure 4 illustrates the performance of BERT and GPT-2 across different ρ values, revealing that ρ significantly affects model performance. Table 6 provides detailed performance for GPT-2 with various ρ values, showing that the SNN accuracy tends to converge as ρ gradually approaches T. When $\rho = T$, the best results are achieved. Furthermore, when T is very small $T \leq 2$, setting $\rho = T$ leads to significant improvements. This indicates

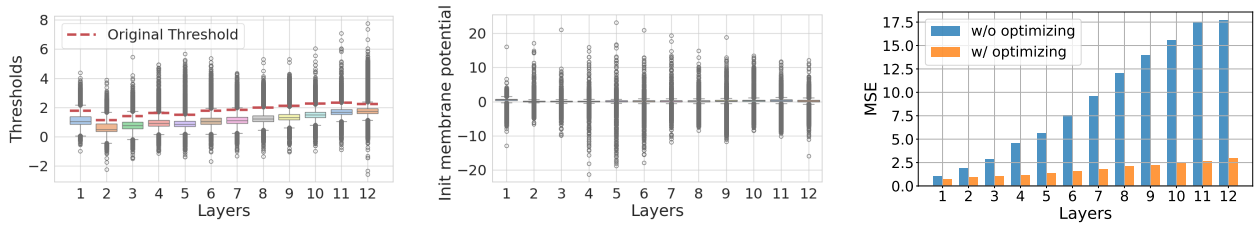

(a) The distribution of thresholds vs. the original threshold over different layers.

(b) The distribution of initial membrane potentials over layers.

(c) Temporal error before and after the optimization over layers.

Figure 5. The effectiveness of the proposed FAS method for threshold and initial membrane potentials optimization.

Table 7. Ablation studies on *LWC* and *NWC*.

LWC	*NWC*	*T=1*	*T=2*	*T=4*	*T=8*	*T=16*
✗	✗	66.41	40.60	48.85	52.19	51.59
✓	✗	64.78	28.99	23.96	22.81	20.22
✗	✓	40.01	23.41	18.30	17.10	16.90
✓	✓	**39.30**	**21.98**	**18.01**	**17.03**	**16.84**

Table 8. Comparison on different L values on Wikitext-103.

L	**ANN**	*T*=1	*T*=2	*T*=4	*T*=8	*T*=16
2	17.89	**20.28**	**18.50**	17.72	17.45	17.41
4	16.87	21.33	18.68	**17.51**	17.10	16.99
8	16.39	23.06	19.30	17.68	**17.03**	**16.84**
16	16.17	25.29	20.64	18.43	17.11	16.90

that FAS can achieve excellent results at low latency. More experiments on BERT are presented in **Appendix G**.

5.5.2. LWC AND NWC OF STAGE 2 :

As described in ***Stage 2***, the proposed FAS method involves Layer-wise calibration (*LWC*) and Neuron-wise calibration (*NWC*). As shown in Table 7, compared to the first row, where none is present, *NWC* and *NWC* can both bring improvement. The performance is the best for every time step when both are present. This indicates *LWC* and *NWC* have a positive impact on the performance of FAS.

5.5.3. PARAMETER L :

To minimize the time steps T, it is intuitive to set L as small as possible. However, setting L too low will reduce the model's capacity, leading to lower accuracy in the converted SNN. As shown in Table 8, increasing L initially can improve the performance of SNN, but causes a performance drop when L reaches 16. Choosing L is a trade-off between achieving high accuracy and maintaining low latency SNN.

Table 9. Comparison of different λ_1, λ_2 values.

$\lambda_1 : \lambda_2$	*T*=1	*T*=2	*T*=4	*T*=8	*T*=16
1:1	**22.80**	19.12	**17.58**	17.14	16.94
1:0	47.06	23.80	18.43	17.36	17.10
0:1	22.80	**19.12**	17.58	17.04	16.89
1:0012	23.06	19.30	17.68	**17.02**	**16.85**

5.5.4. PARAMETER λ_1, λ_2 :

The impact of the weights λ_1, for activation alignment loss, and λ_2, for logits loss (see Eq.10) are shown in Table 9. They do show an impact on accuracy, especially with small time steps. When $T>8$, their impact becomes minor.

5.6. FAS' Effectiveness on Temporal Error

The distributions of thresholds and initial membrane potentials before and after applying ***Stage 2*** are shown in Figure 5a. Most optimized thresholds are lower than their original, with a few outliers. Figure 5b depicts the optimized initial membrane potentials, primarily clustered above 0, with some values exceeding ± 10. We further analyzed the MSE between r_i^l and a^l, as shown in Figure 5c. The MSE reductions in the last four layers are dramatic, 83.95%, 84.42%, 84.8%, and 86.66%, confirming that the proposed adjustments can effectively minimize temporal error.

6. Conclusion

FAS, a fast ANN-SNN conversion method tailored for LLMs, is presented. It aims to leverage the low-cost computing benefits of Spiking LLMs while maintaining high performance. The conversion process is optimized through a two-stage strategy: firstly, full-parameter fine-tuning is applied so training from scratch is not needed. Secondly, a coarse-to-fine calibration strategy is proposed to further minimize conversion errors, particularly temporal errors. Experiments demonstrate that FAS can achieve both high performance and low latency. The evaluation using both

language and vision-language tasks with five LLMs shows that FAS can outperform SOTA approaches, maintaining accuracy comparable to ANN-based models, yet with low time steps. We hereby conclude that FAS is effective for creating Spiking LLMs, offering a promising pathway towards more sustainable neural network-based deep learning.

References

Bai, J., Bai, S., Yang, S., Wang, S., Tan, S., Wang, P., Lin, J., Zhou, C., and Zhou, J. Qwen-vl: A versatile vision-language model for understanding, localization, text reading, and beyond. *arXiv preprint arXiv:2308.12966*, 1(2): 3, 2023.

Bal, M. and Sengupta, A. Spikingbert: Distilling bert to train spiking language models using implicit differentiation. In *AAAI Conference on Artificial Intelligence*, 2023. URL https://api.semanticscholar.org/CorpusID:261049141.

Bal, M. and Sengupta, A. Spikingbert: Distilling bert to train spiking language models using implicit differentiation. In *Proceedings of the AAAI conference on artificial intelligence*, volume 38, pp. 10998–11006, 2024.

Beyer, L., Steiner, A., Pinto, A. S., Kolesnikov, A., Wang, X., Salz, D., Neumann, M., Alabdulmohsin, I., Tschannen, M., Bugliarello, E., et al. Paligemma: A versatile 3b vlm for transfer. *arXiv preprint arXiv:2407.07726*, 2024.

Brown, T., Mann, B., Ryder, N., Subbiah, M., Kaplan, J. D., Dhariwal, P., Neelakantan, A., Shyam, P., Sastry, G., Askell, A., et al. Language models are few-shot learners. *Advances in neural information processing systems*, 33: 1877–1901, 2020.

Bu, T., Ding, J., Yu, Z., and Huang, T. Optimized potential initialization for low-latency spiking neural networks. *ArXiv*, abs/2202.01440, 2022. URL https://api.semanticscholar.org/CorpusID:246485745.

Bu, T., Fang, W., Ding, J., Dai, P., Yu, Z., and Huang, T. Optimal ann-snn conversion for high-accuracy and ultra-low-latency spiking neural networks. *arXiv preprint arXiv:2303.04347*, 2023.

Cao, Y., Chen, Y., and Khosla, D. Spiking deep convolutional neural networks for energy-efficient object recognition. *International Journal of Computer Vision*, 113: 54–66, 2015.

Davies, M., Srinivasa, N., Lin, T.-H., Chinya, G., Cao, Y., Choday, S. H., Dimou, G., Joshi, P., Imam, N., Jain, S., et al. Loihi: A neuromorphic manycore processor with on-chip learning. *Ieee Micro*, 38(1):82–99, 2018.

de Vries, A. The growing energy footprint of artificial intelligence. *Joule*, 2023. URL https://api.semanticscholar.org/CorpusID:264050478.

Deng, S.-W. and Gu, S. Optimal conversion of conventional artificial neural networks to spiking neural networks. *ArXiv*, abs/2103.00476, 2021. URL https://api.semanticscholar.org/CorpusID:232075977.

Devlin, J., Chang, M.-W., Lee, K., and Toutanova, K. Bert: Pre-training of deep bidirectional transformers for language understanding. In *North American Chapter of the Association for Computational Linguistics*, 2019. URL https://api.semanticscholar.org/CorpusID:52967399.

Diehl, P. U., Neil, D., Binas, J., Cook, M., Liu, S.-C., and Pfeiffer, M. Fast-classifying, high-accuracy spiking deep networks through weight and threshold balancing. *2015 International Joint Conference on Neural Networks (IJCNN)*, pp. 1–8, 2015. URL https://api.semanticscholar.org/CorpusID:2676182.

Diehl, P. U., Zarrella, G., Cassidy, A., Pedroni, B. U., and Neftci, E. Conversion of artificial recurrent neural networks to spiking neural networks for low-power neuromorphic hardware. In *2016 IEEE International Conference on Rebooting Computing (ICRC)*, pp. 1–8. IEEE, 2016.

Duan, X., Cao, Z., Gao, K., Yan, W., Sun, S., Zhou, G., Wu, Z., Ren, F., and Sun, B. Memristor-based neuromorphic chips. *Advanced Materials*, 36(14):2310704, 2024.

Dubey, A., Jauhri, A., Pandey, A., Kadian, A., Al-Dahle, A., Letman, A., Mathur, A., Schelten, A., Yang, A., Fan, A., et al. The llama 3 herd of models. *arXiv preprint arXiv:2407.21783*, 2024.

Han et al. Rmp-snn: Residual membrane potential neuron for enabling deeper high-accuracy and low-latency spiking neural network. *2020 IEEE/CVF Conference on Computer Vision and Pattern Recognition (CVPR)*, pp. 13555–13564, 2020. URL https://api.semanticscholar.org/CorpusID:219963592.

Han, B. and Roy, K. Deep spiking neural network: Energy efficiency through time based coding. In *European conference on computer vision*, pp. 388–404. Springer, 2020.

Hao, Z., Bu, T., Ding, J., Huang, T., and Yu, Z. Reducing ann-snn conversion error through residual membrane potential. In *Proceedings of the AAAI Conference on Artificial Intelligence*, volume 37, pp. 11–21, 2023a.

Hao, Z., Ding, J., Bu, T., Huang, T., and Yu, Z. Bridging the gap between anns and snns by calibrating offset spikes. *ArXiv*, abs/2302.10685, 2023b. URL https://api.semanticscholar.org/CorpusID:257050386.

Hinton, G. E., Vinyals, O., and Dean, J. Distilling the knowledge in a neural network. *ArXiv*, abs/1503.02531, 2015. URL https://api.semanticscholar.org/CorpusID:7200347.

Hussain, M. S. The information pathways hypothesis: Transformers are dynamic self-ensembles. In *Proceedings of the 29th ACM SIGKDD Conference on Knowledge Discovery and Data Mining*, pp. 810–821, 2023.

Lee, J., Delbrück, T., and Pfeiffer, M. Training deep spiking neural networks using backpropagation. *Frontiers in Neuroscience*, 10, 2016. URL https://api.semanticscholar.org/CorpusID:2882718.

Li, Y. and Zeng, Y. Efficient and accurate conversion of spiking neural network with burst spikes. In *International Joint Conference on Artificial Intelligence*, 2022. URL https://api.semanticscholar.org/CorpusID:248426984.

Li, Y., Deng, S.-W., Dong, X., Gong, R., and Gu, S. A free lunch from ann: Towards efficient, accurate spiking neural networks calibration. *ArXiv*, abs/2106.06984, 2021. URL https://api.semanticscholar.org/CorpusID:235421730.

Li, Y., Deng, S., Dong, X., and Gu, S. Error-aware conversion from ann to snn via post-training parameter calibration. *International Journal of Computer Vision*, pp. 1–24, 2024.

Lian, S., Shen, J., Liu, Q., Wang, Z., Yan, R., and Tang, H. Learnable surrogate gradient for direct training spiking neural networks. In *IJCAI*, pp. 3002–3010, 2023.

Liu, H., Li, C., Wu, Q., and Lee, Y. J. Visual instruction tuning. *Advances in neural information processing systems*, 36, 2024.

Lozhkov, A., Ben Allal, L., von Werra, L., and Wolf, T. Fineweb-edu, May 2024. URL https://huggingface.co/datasets/HuggingFaceFW/fineweb-edu.

Lv, C., Xu, J., and Zheng, X. Spiking convolutional neural networks for text classification. In *International Conference on Learning Representations*, 2023. URL https://api.semanticscholar.org/CorpusID:259298612.

Lv, C., Li, T., Xu, J., Gu, C., Ling, Z., Zhang, C., Zheng, X., and Huang, X. Spikebert: A language spikformer learned from bert with knowledge distillation, 2024. URL https://arxiv.org/abs/2308.15122.

Merolla, P. A., Arthur, J. V., Alvarez-Icaza, R., Cassidy, A. S., Sawada, J., Akopyan, F., Jackson, B. L., Imam, N., Guo, C., Nakamura, Y., et al. A million spiking-neuron integrated circuit with a scalable communication network and interface. *Science*, 345(6197):668–673, 2014.

Neftci, E. O., Mostafa, H., and Zenke, F. Surrogate gradient learning in spiking neural networks: Bringing the power of gradient-based optimization to spiking neural networks. *IEEE Signal Processing Magazine*, 36(6):51–63, 2019. doi: 10.1109/MSP.2019.2931595.

Radford, A., Wu, J., Child, R., Luan, D., Amodei, D., Sutskever, I., et al. Language models are unsupervised multitask learners. *OpenAI blog*, 1(8):9, 2019.

Rueckauer, B., Lungu, I.-A., Hu, Y., and Pfeiffer, M. Theory and tools for the conversion of analog to spiking convolutional neural networks. *arXiv preprint arXiv:1612.04052*, 2016.

Rueckauer, B., Lungu, I.-A., Hu, Y., Pfeiffer, M., and Liu, S.-C. Conversion of continuous-valued deep networks to efficient event-driven networks for image classification. *Frontiers in neuroscience*, 11:294078, 2017.

Sengupta, A., Ye, Y., Wang, R. Y., Liu, C., and Roy, K. Going deeper in spiking neural networks: Vgg and residual architectures. *Frontiers in Neuroscience*, 13, 2018. URL https://api.semanticscholar.org/CorpusID:3643293.

Shen, G., Zhao, D., Dong, Y., Li, Y., Li, J., Sun, K., and Zeng, Y. Astrocyte-enabled advancements in spiking neural networks for large language modeling. *ArXiv*, abs/2312.07625, 2023. URL https://api.semanticscholar.org/CorpusID:266191693.

Song, X., Song, A., Xiao, R., and Sun, Y. One-step spiking transformer with a linear complexity. In *Proceedings of the Thirty-Third International Joint Conference on Artificial Intelligence*, pp. 3142–3150, 2024.

Sonoda, Y., Kurokawa, R., Nakamura, Y., Kanzawa, J., Kurokawa, M., Ohizumi, Y., Gonoi, W., and Abe, O. Diagnostic performances of gpt-4o, claude 3 opus, and gemini 1.5 pro in "diagnosis please" cases. *Japanese journal of radiology*, pp. 1–5, 2024.

Subramanian, S., Trischler, A., Bengio, Y., and Pal, C. J. Learning general purpose distributed sentence representations via large scale multi-task learning. In *International Conference on Learning Representations*, 2018.

Wang, A., Singh, A., Michael, J., Hill, F., Levy, O., and Bowman, S. R. Glue: A multi-task benchmark and analysis platform for natural language understanding. In *BlackboxNLP@EMNLP*, 2018. URL https://api.semanticscholar.org/CorpusID:5034059.

Wang, Z., Zhang, Y., Lian, S., Cui, X., Yan, R., and Tang, H. Toward high-accuracy and low-latency spiking neural networks with two-stage optimization. *IEEE Transactions on Neural Networks and Learning Systems*, 2023.

Wu, Y., Deng, L., Li, G., Zhu, J., and Shi, L. Spatio-temporal backpropagation for training high-performance spiking neural networks. *Frontiers in Neuroscience*, 12, 2017. URL https://api.semanticscholar.org/CorpusID:6446489.

Xing, X., Zhang, Z., Ni, Z., Xiao, S., Ju, Y., Fan, S., Wang, Y., Zhang, J., and Li, G. Spikelm: Towards general spike-driven language modeling via elastic bi-spiking mechanisms. *arXiv preprint arXiv:2406.03287*, 2024.

Yang, Q., Wu, J., Zhang, M., Chua, Y., Wang, X., and Li, H. Training spiking neural networks with local tandem learning. *Advances in Neural Information Processing Systems*, 35:12662–12676, 2022.

Yao, M., Hu, J., Zhou, Z., Yuan, L., Tian, Y., Xu, B., and Li, G. Spike-driven transformer. *Advances in neural information processing systems*, 36, 2024a.

Yao, M., Richter, O., Zhao, G., Qiao, N., Xing, Y., Wang, D., Hu, T., Fang, W., Demirci, T., De Marchi, M., et al. Spike-based dynamic computing with asynchronous sensing-computing neuromorphic chip. *Nature Communications*, 15(1):4464, 2024b.

Zenke, F. and Vogels, T. P. The remarkable robustness of surrogate gradient learning for instilling complex function in spiking neural networks. *Neural computation*, 33(4): 899–925, 2021.

Zhang, S., Roller, S., Goyal, N., Artetxe, M., Chen, M., Chen, S., Dewan, C., Diab, M., Li, X., Lin, X. V., et al. Opt: Open pre-trained transformer language models. *arXiv preprint arXiv:2205.01068*, 2022.

Zhu, D., Chen, J., Shen, X., Li, X., and Elhoseiny, M. Minigpt-4: Enhancing vision-language understanding with advanced large language models. *arXiv preprint arXiv:2304.10592*, 2023a.

Zhu, R.-J., Zhao, Q., Li, G., and Eshraghian, J. K. Spikegpt: Generative pre-trained language model with spiking neural networks. *arXiv preprint arXiv:2302.13939*, 2023b.

A. The Spike Rate of SNNs

This section present the details to get the functional representation of spike rate. First, as indicated in Subsection 3.2, the kinetic behavior of IF neuron can be represented by Eq. (11):

$$\boldsymbol{v^l(t)} = v^l(t-1) + W^l S^{l-1}(t)\theta^{l-1} - S^l(t)\theta^l, \tag{11}$$

where $v^l(t)$ represent the membrane potential at time steps t in the i-th layers. W^l and θ^l are the weight matrix and firing threshold of the IF neuron, respectively. $S^l(t)$ denotes the transmission of discrete spikes at the l-th layer at time steps t. Note that when $v^l(t-1)+W^l S^{l-1}(t)\theta^{l-1}$ exceeds the threshold θ^l, the IF neuron is fired, and $S^l(t)$ equals to 1. Otherwise, the IF neuron is muted and $S^l(t)$ equals to 0.

By accumulating Eq. (11) over time steps 1 to T, the spike rate $r^l(T)$ of layer l can be obtained by Eq. (12):

$$r^l(T) = W^l r^{l-1}(T) + (-\frac{v^l(T) - v^l(0)}{T}). \tag{12}$$

It can be seen from the formula that r^l and r^{l-1} have a linear relationship, similar to the activation function in ANNs. Therefore, we can map the activation value a^l of analog neurons in ANNs to r^l of IF neurons in SNNs. When $0 < v^l(T) < \theta^l$ and $W^l r^{l-1}(T) \in (0, \theta^l)$, Eq. (12) can be approximated as below in Eq. (13):

$$r^l(T) = \frac{\theta^l}{T}\left\lfloor \frac{TW^l r^{l-1}(T) + v^l(0)}{\theta^l} \right\rfloor. \tag{13}$$

Finally, combining the situation $W^l r^{l-1}(T) \notin (0, \theta^l)$, the spike rate r^l of IF neurons at layer l can be represented as a continuous step function, as shown in Eq. (14):

$$r^l(T) = \text{clip}(\frac{\theta^l}{T}\left\lfloor \frac{TW^l r^{l-1}(T) + v^l(0)}{\theta^l} \right\rfloor, 0, \theta^l). \tag{14}$$

B. Algorithm Details of FAS

The detailed steps of FAS are in Algorithm 1. Lines 2-4 are the processes of ***Stage 1***, addressing QC errors through full-parameter fine-tuning. More specifically, it starts by replacing the activation function with QCFS (Line 2) and fine-tuning the model on the datasets D and $\hat{D}$ (Line 3). Subsequently, the weights are transferred from the fine-tuned ANN model to the SNN model (Line 4). Lines 6-11 describe ***Stage 2***, which employs a layer-wise and neuron-wise coarse-to-fine calibration optimization strategy. Each layer undergoes layer-wise calibration (Line 7) followed by neuron-wise calibration on mini-batches sampled from $\hat{D}$ (Line 10).

Algorithm 1 Overall Framework of FAS

Input: Pre-trained ANN model f_{ANN} , Finetuning Dataset D, Downstream Dataset $\hat{D}$, Calibration steps ρ.
Output: SNN model f_{SNN}.

1: /* ***Stage 1:*** **Eliminate QC Errors** */
2: Replace Activation function with QCFS in f_{ANN};
3: Full-parameter fine-tuning with D and $\hat{D}$;
4: Copy weights from f_{ANN} to the SNN f_{SNN};
5: /* ***Stage 2:*** **Eliminate Temporal Error** */
6: **for** each layer of f_{SNN} **do**
7: Perform the proposed *layer-wise calibration* strategy for the l-th layer;
8: **end for**
9: **for** each minibatch $\hat{D}'$ sampled from $\hat{D}$ **do**
10: Perform the proposed *neuron-wise calibration* strategy on $\hat{D}'$;
11: **end for**
12: **return** f_{SNN}.

C. Datasets

This is the supplementary for Section Datasets & Baselines. For NLU tasks, we chose seven different types of tasks, i.e., six classification and one regression tasks, from the GLUE benchmark. We selected Quora Question Pair (QQP) and Microsoft Research Paraphrase Corpus (MRPC) for classification tasks, and Semantic Textual Similarity Benchmark (STSB) for regression task to evaluate our FAS on similarity and paraphrase tasks. For inference tasks, we opted for MultiGenre Natural Language Inference (MNLI), Question Answering NLI (QNLI), and Recognizing Textual Entailment (RTE) datasets. For single-sentence-based sentiment analysis tasks, we chose Stanford Sentiment Treebank (SST-2).

For NLG task, we chose the following two classic text classification datasets, i.e., Enwik8 and WikiText-103, to evaluate the text generation performance of FAS. Specifically, the Enwik8 dataset is a large-scale text dataset consisting of the first 100 million characters from Wikipedia. It is widely used for character-level language modeling and text generation tasks, providing a challenging benchmark for models due to its extensive and varied content. The Bit-Per-Byte (BPB) metric is commonly employed to assess its performance. In addition, the WikiText-103 dataset is another comprehensive text dataset derived from Wikipedia articles. It contains over 100 million words and is known for its high-quality, naturally occurring text. WikiText-103 is commonly used for training and evaluating language models, particularly in tasks involving text generation, language modeling, and machine translation. Perplexity (PPL) is the metric of choice for evaluating the performance.

For vision-language tasks, several key benchmarks are widely used. BLINK is a benchmark for multimodal language models, consisting of 14 classic computer vision tasks reformatted into 3,807 multiple-choice questions. It is designed to evaluate visual perception abilities such as relative depth estimation, visual correspondence, forensics detection, and multi-view reasoning. HallusionBench, on the other hand, focuses on image-context reasoning in large visual-language models. It contains 346 images paired with 1,129 expert-crafted questions, assessing logical consistency, response tendencies, and failure modes like language hallucination and visual illusion. MMMU is another crucial benchmark for evaluating multimodal models on advanced, college-level tasks. With 11.5K questions across six core disciplines, 30 subjects, and 183 subfields, it tests perception and reasoning with domain-specific knowledge across 32 heterogeneous image types, including charts, diagrams, maps, and chemical structures.

D. Baselines

Following Section Datasets & Baselines, we selected various SOTA baseline models to verify the effectiveness of our FAS on NLU and NLG tasks.

NLU tasks - The baselines are as follows:

- CBoW (Wang et al., 2018): CBoW is a simple sentence representation technique that averages the GloVe embeddings of individual words, ignoring syntactic structure and contextual dependencies.
- BiLSTM (Wang et al., 2018): BiLSTM combines LSTM networks with a bidirectional structure to capture both past and future context in sequences
- BiLSTM+Attn (Wang et al., 2018): BiLSTM+Attn combines BiLSTM's sequence understanding with Attention's focus on relevant sentence parts.
- GenSen (Subramanian et al., 2018): GenSen is a multi-task learning framework that combines diverse objectives to learn general-purpose sentence representations, leading to improved performance on various NLP tasks.
- SNN-TextCNN (Lv et al., 2023): It is a variant of the TextCNN that combines spiking neural networks.
- BERT (Devlin et al., 2019): BERT is a bidirectional language model based on the Transformer Encoder-only architecture and an auto-encoding training paradigm.
- spikeBERT (Lv et al., 2024): It transfers knowledge from the transformer-based BERT model to the spiking neuron-based architectures with knowledge distillation.
- SpikeLM (Xing et al., 2024): SpikeLM is a novel language model based on SNN that addresses the performance limitations of traditional SNNs in language tasks. By employing an elastic bi-spiking mechanism, SpikeLM achieves

competitive performance with deep neural networks on various language tasks while maintaining the energy efficiency of SNNs.

- spikingBERT (Bal & Sengupta, 2023): SpikingBERT proposes a novel bioinspired spiking language model. which leverages the average spiking rate of neurons at equilibrium to train a neuromorphic spiking LM using implicit differentiation technique.
- OPT (Zhang et al., 2022): The OPT (Open Pre-trained Transformers) model is a suite of decoder-only pre-trained transformers ranging from 125 million to 175 billion parameters, designed to match the performance and sizes of GPT-3 models while promoting reproducible and responsible research at scale.

NLG tasks - The selected baselines are as follows:

- spikeGPT (Zhu et al., 2023b): It explores combining the powerful Transformer architecture with SNN by utilizing linearization and recurrent Transformer blocks..
- AstroSNN (Shen et al., 2023): AstroSNN integrates neuron-astrocyte interactions into the computational paradigm, demonstrating broad applicability across various hardware platforms and narrowing the gap between biological plausibility and neural modeling.
- GPT-2 (Radford et al., 2019): It is a Transformer-based deep learning model that leverages self-attention for text dependency parsing and excels in text generation and understanding post-pre-training on extensive data.

Vision-Language tasks - The chosen baselines are as follows:

- MiniGPT-4-v2-7B (Zhu et al., 2023a): MiniGPT-4 is a vision-language model that aligns a frozen visual encoder with a frozen large language model (Vicuna) using a single projection layer, demonstrating advanced multi-modal capabilities with high computational efficiency.
- Qwen-VL-8B (Bai et al., 2023): Qwen-VL is a large-scale vision-language model series that enhances the Qwen-LM foundation with visual capabilities, enabling advanced multi-modal tasks like image captioning, question answering, and visual grounding, setting new benchmarks in both generalist and dialog-based tasks.
- Claude 3 (Sonoda et al., 2024): Claude 3 is a family of advanced AI models, including Haiku, Sonnet, and Opus, offering progressively higher intelligence, speed, and cost-efficiency, excelling in tasks like expert knowledge, mathematics, content creation, and multilingual conversation.
- LLaVA-1.5-7B (Liu et al., 2024): LLaVA 1.5 is an advanced vision-language model that builds on the previous LLaVA model by improving performance in image captioning, visual question answering, and other vision-language tasks. It integrates large language models with powerful vision encoders, enhancing its ability to process and understand both text and images. This model also benefits from a more robust training framework, leveraging large, diverse datasets and fine-tuning strategies to increase its generalization capabilities across a wide range of multimodal tasks.
- PailGemma-3B (Beyer et al., 2024): PaliGemma is an open Vision-Language Model (VLM) that is based on the SigLIP-So400m vision encoder and the Gemma-2B language model. It is trained to be a versatile and broadly knowledgeable base model that is effective to transfer. It achieves strong performance on a wide variety of open-world tasks.

For ANN-SNN conversion methods, the chosen baselines are as follows:

- SPR (Hao et al., 2023a): It theoretically establishes the mathematical relationship between residual membrane potential and the specific case of unevenness error, and propose an optimization strategy based on residual membrane potential to reduce unevenness error.
- QCFS (Bu et al., 2023) : It theoretically analyzes ANN-SNN conversion error and derive the estimated activation function of SNNs. Then it proposes the quantization clipfloor-shift activation function to replace the ReLU activation function in source ANNs, which can better approximate the activation function of SNNs.
- COS (Hao et al., 2023b): It proposes a method to judge offset spike based on the residual membrane potential and an optimization method to eliminate conversion errors by shifting the initial membrane potential.

Table 10. Training and fine-tuning hyperparameters for BERT and GPT-2. * denotes the learning rate for the threshold and initial membrane potential. ** denotes the learning rate for all parameters except the threshold and initial membrane potential. † denotes 1 epoch for the Enwik8 dataset and 3 epochs for the WikiText-103 dataset.

Stage	Model	Dataset	Learning Rate*	Learning Rate**	BatchSize	Epochs/Tokens
Stage 1	**BERT**	WikiText-103	0.01	5×10^{-5}	32	3 epochs
	BERT	Downstream Tasks	0.01 - 0.08	2×10^{-5} to 6×10^{-5}	32	3 epochs
	GPT-2	FineWeb-Edu	0.001	9×10^{-5}	16	0.3 billion tokens in 1 epoch
	GPT-2	Downstream Tasks	0.005	1.2×10^{-4}	8	1 epochs / 3 epcoh †
Stage 2	**BERT**	Downstream Tasks	0.01 -0.06	-	16	3 epochs
	GPT-2	Downstream Tasks	0.005	-	2	1 epochs / 3 epcoh †

E. Experiment Settings

This section supplements the section of Datasets & Baselines. To conserve GPU memory, we employed DeepSpeed's ZeRO-2 optimization, utilizing mixed-precision computation on two Nvidia RTX 3090 GPUs, each with 24GB of memory. For stability, gradient clipping was applied with a threshold of 1. The AdamW optimizer was used throughout.BERT was fully fine-tuned on the WikiText-103 dataset, whereas GPT-2 was trained on 0.3 billion tokens from the FineWeb-Edu dataset (Lozhkov et al., 2024).

For downstream tasks, we utilized the respective task's training dataset. In the absence of a standard split, we followed the convention (Lv et al., 2023), randomly selecting 10% of the samples as the test set. The hyperparameters were set as follows: $\alpha^l = 0.6$ and $\beta^l = 0.1$ for both BERT and GPT-2, $\lambda_1 = 1$ and $\lambda_2 = 0.0012$ for GPT-2, and $\lambda_1 = 1$ with λ_2 ranging from 0.2 to 1 in increments of 0.1, selecting the optimal result.

More detailed settings of the learning rate and epochs for each task are presented in Table 10. More specifically, in stage 1, BERT is initially trained on the WikiText-103 dataset used a threshold learning rate of 0.01 and other parameters set at 5×10^{-5}, over 3 epochs. Fine-tuning on downstream tasks adjusted the threshold learning rate between 0.01 and 0.08, with other parameters ranging from 2×10^{-5} to 6×10^{-5}. In addition, GPT-2 is trained on the FineWeb-Edu dataset and used a threshold learning rate of 0.001. Other parameters in training GPR-2 are set at 9×10^{-5}, covering 0.3 billion tokens in 1 epoch. Fine-tuning on WikiText-103 set the threshold learning rate to 0.005 and other parameters to 1.2×10^{-4}. In stage 2, the learning rate of BERT is ranged from 0.01 to 0.06, depending on the convention of different downstream tasks. Furthermore, the learning rate of GPT-2 is set to 0.005 on the WikiText-103 dataset.

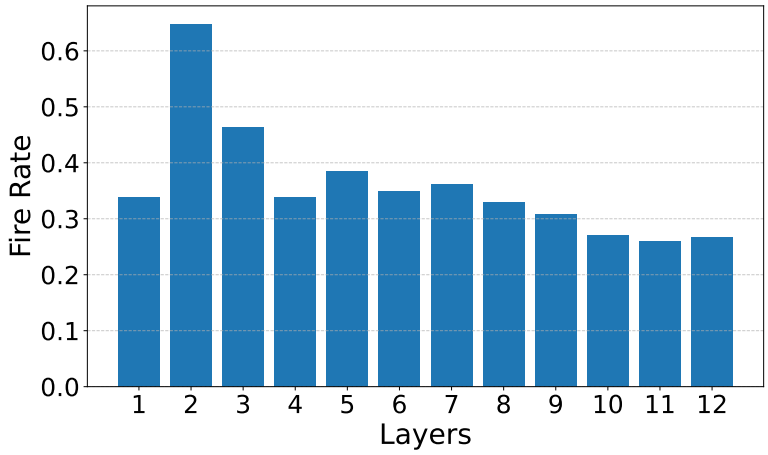

Figure 6. Firing rate visualization of GPT-2.

Table 11. Performance and energy usage of converted SNNs relative to ANN for GPT-2. Note that 'Per. Deg.' means the 'Performance Degradation'. Also, SRP and COS need an additional 16 time steps to gather the necessary prior information.

Model	Per. Deg.	FAS		QCFS		SRP		COS	
		Perplexity	**Energy (%)**	**Perplexity**	**Energy (%)**	**Perplexity**	**Energy (%)**	**Perplexity**	**Energy (%)**
GPT-2	**ANN (0)**	16.53	100	16.53	100	16.53	100	16.53	100
	$\downarrow(0-1)$	$16.84_{\mathbf{T=16}}$ $17.02_{\mathbf{T=8}}$	28.19 14.21						
	$\downarrow(1-2)$	$17.68_{\mathbf{T=4}}$	7.04						
	$\downarrow(2-3)$	$19.27_{\mathbf{T=2}}$	3.99			$19.41_{\mathbf{T=16}}$	36.13	$19.16_{\mathbf{T=16}}$ $19.36_{\mathbf{T=8}}$	35.99 27.11
	$\downarrow(>3)$	$23.02_{\mathbf{T=1}}$	2.19	$19.64_{\mathbf{T=16}}$ $20.19_{\mathbf{T=8}}$ $21.20_{\mathbf{T=4}}$ $22.48_{\mathbf{T=2}}$ $29.04_{\mathbf{T=1}}$	17.90 8.99 4.52 2.26 1.00	$19.74_{\mathbf{T=8}}$ $20.36_{\mathbf{T=4}}$ $21.27_{\mathbf{T=2}}$ $26.71_{\mathbf{T=1}}$	27.08 22.53 20.22 18.93	$19.86_{\mathbf{T=4}}$ $20.81_{\mathbf{T=2}}$ $26.38_{\mathbf{T=1}}$	22.67 20.43 19.17

F. Analysis of Power & Energy Efficiency

Since the converted model still involves MAC operations, we focused our comparison solely on the energy consumption of the spiking parts and their corresponding parts in the ANN. Specifically, synaptic operations in SNNs vary depending on spike sparsity with sparse accumulation (AC). In contrast, synaptic operations involving multiplication and accumulation (MAC) in ANNs remain constant within a defined network structure. We measure floating-point AC and MAC operations, using 0.9 pJ per AC and 4.6 pJ per MAC, as reported in (Li et al., 2021).

To quantitatively assessrgy savings, we compare our converted GPT-2 with their ANN counterparts (Merolla et al., 2014) in terms of performance and energy consumption. Table 11 lists the results relative to those of ANN in percentiles for FAS and SOTA ANN-SNN conversation methods QCFS, SRP and COS. On the GPT-2 model, FAS outperforms other ANN-SNN conversion methods in terms of accuracy. In the case of GPT-2, FAS can achieve similar ANN performance with time steps 2, 4 & 8. Other methods could not go above the category of "2-3" of performance drop, e.g., the increase in perplexity.

Then, we visualize the sparsity of our optimized SNN as shown in Fig. 6, which illustrates the spike rate of all layers of the GPT-2 model using the WikiText-103 dataset with $T = 4$. A spike rate of 1 means that the numbers of operations in the ANN and SNN are identical. Fig. 6 reveals that the maximum spike rate observed is below 0.64, while the minimum is around 0.25. This suggests that our FAS-generated SNN can significantly reduce the required operations compared to the ANN counterpart.

The analysis of power and energy efficiency demonstrates the following:

1. **FAS achieves SOTA performance across all time steps, surpassing the LLM.** In particular, the accuracy of FAS with 16 time steps using the BERT model exceeds that of its ANN counterpart and other SOTA methods.

2. **FAS runs fast, especially under similar energy consumption.** For example, on GPT-2 models, the energy consumption of FAS and QCFC is 7.04% and 8.99% under 4 and 8 time steps, respectively. As a result, FAS achieves lower perplexity, and the reduced number of time steps results in faster inference times.

Table 12. Impact of the parameter ρ in BERT. Baseline refers to the SNN without Stage 2 optimization.

Method	**Model**	**ANN**	T=1	T=2	T=4	T=6	T=8	T=16	T=32
Baseline	BERT	90.88	81.10	81.97	84.97	85.99	86.63	87.39	87.74
FAS ($\rho = 1$)	BERT	90.88	**88.96**	89.27	89.46	89.93	89.97	89.95	89.99
FAS ($\rho = 2$)	BERT	90.88	88.63	**89.62**	**90.61**	**90.83**	**90.94**	**90.74**	90.57
FAS ($\rho = 4$)	BERT	90.88	62.94	88.52	90.13	90.42	90.63	90.66	**90.77**
FAS ($\rho = 6$)	BERT	90.88	50.54	86.91	90.12	90.39	90.46	90.65	90.66
FAS ($\rho = 8$)	BERT	90.88	50.54	66.83	89.35	89.88	90.43	90.55	90.63

G. The Impacts of Parameter ρ on BERT

We examine the effect of the hyperparameter calibration steps ρ in ***Stage 2*** of FAS. Table 12 shows performance of BERT with different values of ρ. It is evident that ρ significantly influences performance. When $\rho = 2$, BERT consistently achieves better results across all time steps. Notably, at $T = 8$, it reaches an accuracy of 90.94%, surpassing the 90.88% accuracy of ANN, demonstrating the near-lossless conversion capability of FAS.